國 立 中 央 大 學

Physics Department
Master thesis

VUV and EUV irradiation of CH_4+NH_3 ice mixtures

- An implication of Tholin on Charon

研究生: Leung Pui Shan

指導教授: Chen Yu Jung

November 2017

國立中央大學圖書館
碩博士論文電子檔授權書

本授權書授權本人撰寫之碩/博士學位論文<u>全文電子檔</u>(不包含紙本、詳備註 1 說明)，在「國立中央大學圖書館博碩士論文系統」。(以下請擇一勾選)

( )<u>同意</u> (立即開放)

( )<u>同意</u> (請於西元 ＿＿＿＿年＿＿月＿＿日開放)

( )<u>不同意</u>，原因是：＿＿＿＿＿＿＿＿＿＿＿＿＿＿＿

在國家圖書館「臺灣博碩士論文知識加值系統」

( )<u>同意</u> (立即開放)

( )<u>同意</u> (請於西元 ＿＿＿＿年＿＿月＿＿日開放)

( )<u>不同意</u>，原因是：＿＿＿＿＿＿＿＿＿＿＿＿＿＿＿

以非專屬、無償授權國立中央大學、台灣聯合大學系統圖書館與國家圖書館，基於推動「資源共享、互惠合作」之理念，於回饋社會與學術研究之目的，得不限地域、時間與次數，以紙本、微縮、光碟及其它各種方法將上列論文收錄、重製、與利用，並得將數位化之上列論文與論文電子檔以上載網路方式，提供讀者基於個人非營利性質之線上檢索、閱覽、下載或列印。

研究生簽名: ＿＿＿＿＿＿＿＿＿＿ 學號：＿＿＿＿＿＿＿＿＿＿

論文名稱:＿＿＿＿＿＿＿＿＿＿＿＿＿＿＿＿＿＿＿＿＿＿＿

指導教授姓名：＿＿＿＿＿＿＿＿＿＿＿＿＿＿＿

系所 ：＿＿＿＿＿＿＿＿＿＿所 ☐<u>博士班</u> ☐<u>碩士班</u>

備註：
1. 本授權書之授權範圍僅限電子檔，紙本論文部分依著作權法第 15 條第 3 款之規定，採推定原則即預設同意圖書館得公開上架閱覽，如您有申請專利或投稿等考量，不同意紙本上架陳列，須另行加填聲明書，詳細說明與紙本聲明書請至 http://thesis.lib.ncu.edu.tw/ 下載。
2. 本授權書請填寫並**親筆**簽名後，裝訂於各紙本論文封面後之次頁（全文電子檔內之授權書簽名，可用電腦打字代替）。
3. 請加印一份單張之授權書，填寫並親筆簽名後，於辦理離校時交圖書館（以統一代轉寄給國家圖書館）。
4. 讀者基於個人非營利性質之線上檢索、閱覽、下載或列印上列論文，應遵守著作權法規定。

_____ / _____

_____
( )

_____ ( )

___ ___ ___

_____   /   _____

_____

_____

_____

_____

_____

_____

VUV and EUV irradiation of CH$_4$+NH$_3$ ice mixtures

- An implication of Tholin on Charon

中文摘要

關鍵字： 碩博士論文，體裁檔，LaTeX，XeLaTeX

　　此論文範例得以完成是由於體裁檔(ncuthesis.cls)的完成。期間多方閱讀、吸收、漸有所獲，直至發掘兩篇網路文章，深入了解後再加入中文化及適當增修而成。本體裁檔可再增修，複製，直接採用做個人用途，或供單位使用，唯不可做商業用途。

　　此套件係自助編寫屬非賣品，可自由使用，但不做任何保證。期望提供學生便利性，做出符合國立中央大學所規範的研究所論文格式，但不隱含任何商業價值。Open NCU Thesis Requirements

來源

https://code.google.com/p/ncu-thesis-latex-template/

功能

- 論文格式滿足本校要求。

- Uncode/UTF8 中文化。

- 可選擇編譯方式(pdfLaTeX，XeLaTeX)。

- 可選單面印刷或雙面印刷。

- 快速編譯及越界偵錯。

- 可列印紙張結構及參數。

- 顯示智財權及製作日期。

- 具索引及浮水印功能。

- 其它文書製作及提醒功能。

- 如何使用體裁檔請看第一章說明。

- 如何使用LaTeX 請看第二章說明。

- 如何製作參考文獻請看第三章說明。

VUV and EUV irradiation of CH_4+NH_3 ice mixtures

- An implication of Tholin on Charon

英文摘要

Keywords: Master/Doctorial thesis, Class file, LaTeX, XeLaTeX

The files included in the directiory are free to use, copy, or modify for personal use or within an organization. Primarily, the files are for graduates who want to write their theses in LaTeX/XeLaTeX and meet the requirements stipulated by the National Central University.

This document is distributed in the hope that it will be useful to graduates, but without any warranty; without even the implied warranty of merchantability.

Source

https://code.google.com/p/ncu-thesis-latex-template/

Features

- Master/Doctorial thesis stipulated by National Central University.

- Unicode/UTF8 supports.

- Compilable by pdfLaTeX or XeLaTeX.

- Oneside or twoside printing.

- Fast compilation and overfull detection.

- Page layout and parameters.

- Copyright and time stamp.

- Index, watermark capabilities.

- Other thesis variants and todonote reminder.

- How to use this package —— Chapter 1.

- How to use LaTeX (very brief) —— Chapter 2.

- How to generate references —— Chapter 3.

VUV and EUV irradiation of CH_4+NH_3 ice mixtures

- An implication of Tholin on Charon

謝誌

體裁檔受啓發於兩位英美教授於網路上的文章，並經吾人中文化及適當增修而成。本體裁檔可再增修，複製，直接採用做個人用途，或單位使用，唯不可做商業用途。請尊重上述兩位教授的無私奉獻。

- 感謝TeX/LaTeX網路社群內，龐大的TeX/LaTeX社群及其網頁提供無價資訊。

- 欣逢中央大學教務處註冊組組長，蕭嘉璋老師，見微知著，並予協助，僅此誌謝。

- 承蒙太空及遙測研究中心蔡富安老師協助在Ubuntu 12.04上 TeXLive-2009測試成功，僅此誌謝。

- 2013/06/13碩士班 葉信麟同學發現目錄頁碼不正確。

- 2013/07/04碩士班 林億同學發現附錄節碼不正確。

Contents

List of Figures

List of Tables

1. Methods

1.1 Laboratory Astrophysics

To study the chemical reactivity in astrophysical environment experimentally, we conducted our experiments in Interstellar photoprocessing system (IPS) [?], an ultrahigh vacuum chamber with base pressure 3×10^{-10} torr and 14 K, corresponds to a density of 10^6 cm^{-3}, similar to dense cloud interiors. The system will be introduced in detail in section 1.1.1. To simulate the irradiation in interstellar environments, we use a micro-wave discharge hydrogen lamp (MDHL) and monochromatic extreme-ultraviolet irradiation (EUV) 30.4 nm to irradiate our ice mixtures, and they will be introduced in section 1.1.2 and 1.1.3 respectively. The experimental protocols will be elaborated in section 1.2. In order to better understand the physics behind, some basic theories of Infrared spectroscopy and concepts of chemical kinetics used in data analysis are included in section 1.3 and 1.4 respectively.

1.1.1 Experimental simulations by IPS system

We conducted our astrophysical simulations in Interstellar Photo Processing System (IPS) (figure 1.1). IPS consists in three systems: the main chamber, where our experiments take places; the detection system, where we collect our data; and a gasline system, where we prepare our samples.

The main system consists of an ultrahigh vacuum chamber equipped with a closed-cycle helium cryostat (CTI-M350). It is pumped by a turbo molecular pump (KTKT FF – 160/620ZE, capacity 600 liters s^{-1}), which is backed up by a scroll pump, and a non –evaporation getter pump. The getter pump is a powerful tool to adsorb residue gases inside the main chamber, with a larger surface area, H$_2$, CO and N$_2$ are
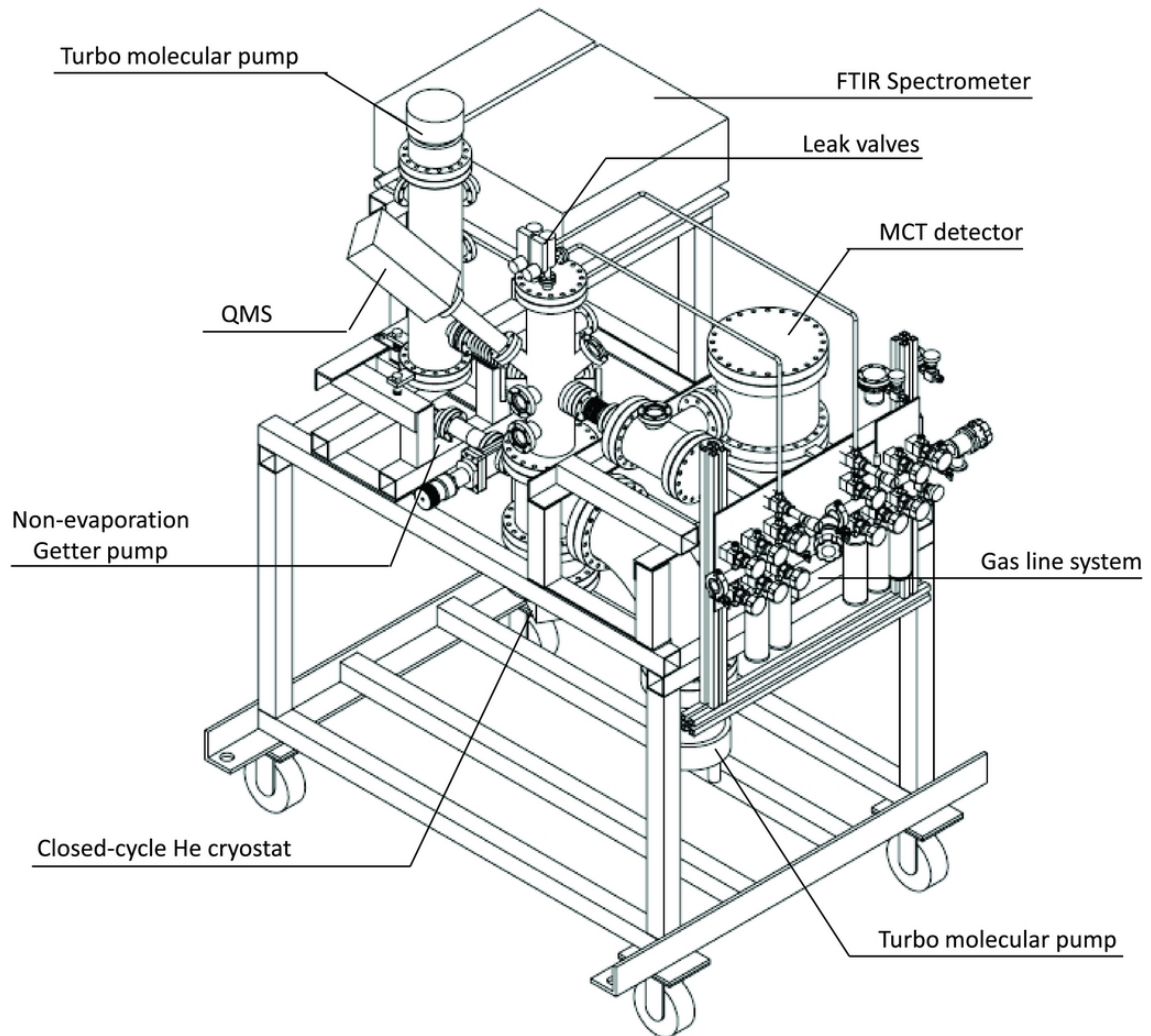
Figure 1.1: The schematic diagram of IPS system, mechanical pumps are not shown for clarity. (Quoted from Chen et al. 2014)

adsorbed to obtain a better base pressure. After baking, the base pressure of our main chamber can reach 1×10^{-10} torr at 14 K, monitored by a Granville-Phillips 370 Stabil-Ion gauge. This pressure can be used to demonstrate the dense cloud interior environments and star forming region. The substrate we have chosen is KBr, which can allow infra-red photons with 700 to 4000 cm^{-1} to penetrate. It is mounted by substrate holder made of oxygen-free copper, on the second stage of cold finger mounted on the tip of cryostat. Two silicon diodes and also a heater were placed onto the cold finger and one of the silicon diodes is near the substrate holder. They were connected to a temperature controller and PID system to achieve a warmup rate of 1K/min with an accuracy of 0.1 K.

The detection system consists in a mid-infrared Fourier transform spectrometer (mid-FTIR) (ABB FTLA2000-104) and a Quadrupole Mass Spectrometer (QMS). To prevent absorption bands of CO, CO_2 and H_2O gas in the atmosphere, the IR beam path was built inside vacuum, pumped by dry pump. The main chamber and the IR path are separated by ZnSe windows, which can allow infra-red penetration from 0.5 – 20 um with absorption less than 0.07 %. In this study, the infrared spectra are obtained with resolution of 4 cm^{-1} and averaged over 32 scans. The angle between the IR beam path and the substrate holder is 45 degrees. The QMS (MKS Microvision 2) consists of a controller and mechanical part sealed by a mounting flange in ultrahigh vacuum. It is mounted 10 cm from the substrate and run with a resolution 0.5 a.m.u. The Ionizer release 70 eV electron by filament and ionize incoming molecules to positive charged ions between anode grid and repeller. The ions were accelerated by focus plate and enters ion filter, which consists of four circular rods, with a combination of A.C and D.C. potential to sieve whole bandpass ions at millisecond timescale. The selected ions enter ion detector and are detected by either faraday cup and continuous dynode electron multiplier (CDEM) which can secondary multiply weak signals.

The samples are prepared in situ in our gasline system. It contains four stainless steel bottles with the same volume, which is used to deter-
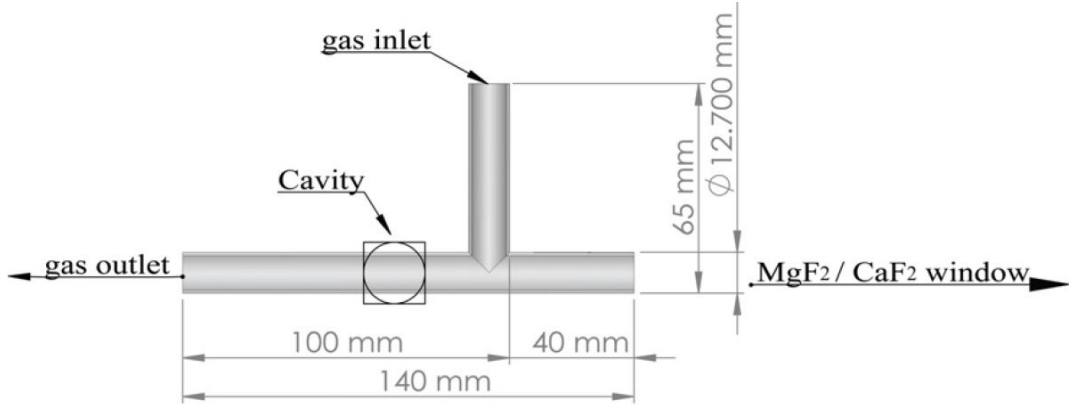
Figure 1.2: The cross-section of MDHL (T-type geometry) (Quoted from Chen et al. 2014).

mine relative proportion of the gas mixtures by their partial pressures. The ammonia gas 99.99 % and methane 99.999 % are mixed with partial pressure measured by a Baratron with 0 - 100 torr range with a 0.25

1.1.2   Vacuum-UV source

In order to simulate the photoprocessing of vacuum ultraviolet (VUV) irradiation onto the interstellar ices and ices on planetary bodies, including KBOs, the ice mixtures are irradiated with a T-type Microwave-Discharged Hydrogen-flow lamp (MDHL). The molecular hydrogen with pressure 0.4 torr flows through the lamp with a support of a mechanical pump. Using a 2.4 GHz microwave generator and high voltage discharge, a low pressure plasma is produced in the Evenson cavity. Figure 1.2 shows a cross-section of T-type quartz tube; the middle part of the T-type quartz tube is being tunned by a ceramic rod that is called Evenson cavity. In order to measure the photon flux in situ, we use an 88 % transmittance nickel mesh with its photoelectric efficiency being obtained by high-flux beamline in National Synchrotron and a SXUV 100 photodiode calibrated by NIST. A MgF_2 window is placed between the lamp and the sample holder to prevent penetration of VUV photons with wavelength shorter than 114nm, leads to a cut off at 114nm. Figure 1.3 shows a VUV emission spectrum of a MDHL. It consists in Ly-α (121.6nm) and H_2 molecular emission in 110-180 nm range. Chen et al. (2014) showed that the spectral characteristics of the VUV light emitted in this range depends on the gas type (mixture of

4
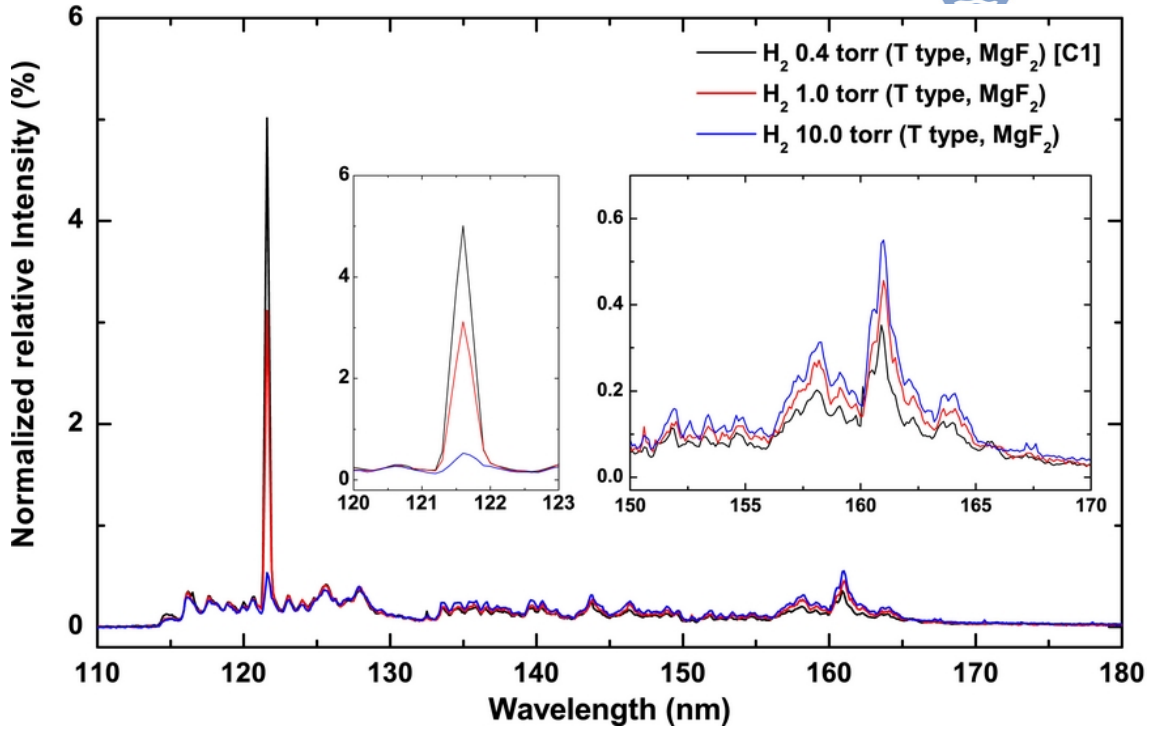
Figure 1.3: VUV spectra of MDHL (T-type geometry, 110-180 nm) with different H_2 pressure inside the lamp(Quoted from Chen et al. 2014).

H_2 with He or Ar etc), pressure of H_2 and lamp geometry. Throughout those configurations stated there, we adopted 0.4 torr molecular hydrogen and T-type MDHL that produces VUV irradiation at 114-170 nm with 19.1 % of Ly-α and a mean photon energy of 9.27 eV. The photon flux is 6.4×10^{13} photons $cm^{-2}s^{-1}$ at sample position.

1.1.3 Extreme EUV source

To simulate the solar EUV irradiation reflected by IPM on both Charon and interstellar ices, we use the HF-CGM high – flux beam line of the National Synchrotron Radiation Research Center in Hsinchu, Taiwan. It provides a continuum EUV to VUV photons from 4 to 40 eV. The continuum is separated into monochromatic 30.4nm photons with a six-meter cylindrical grating monochromter with an incident angle of 70 degrees. With the help of a movable entrance slit and movable curved exit slit, the energy resolving power can reach around 3×10^4 at 40 eV for grating 1600 l/mm with both slits movable and set opening to 10 μm [?]. Similar to VUV irradiation provided by MDHL, the light intensity was monitored by the same nickel mesh with photoelectric

efficiency obtained by SXUV 100 photodiode calibrated by NIST. With the known photoelectric efficiency, the flux of monochromatic 30.4nm is measured to be 2.15×10^{14} photons $s^{-1}cm^{-2}$ with a spot size of 1 cm

1.2   Experimental Protocol

In this section, we will briefly introduce the procedures of how we performed our experiments. It is divided into four parts, preparation and cooling, deposition, irradiation and warmup.

Preparation of experiments and cooling

Before any of experiment is done, we bake our system at 100 oC for 48 hours to reduce the contamination of water and residue gases as much as possible. It was cooled to room temperature that the background pressure can reach routinely at 1×10^{-10} torr. The gasline were connected with the regulators of the gas tanks and bake to 100 ^oC and pumped by moleculaturbo pump for two days before any experiment were done. Also, The water sample has been freeze thaw several times by liquid nitrogen until there is no pressure increase recorded by baratron when water is freezed. Before cooling the substrate to cryogenic temperature, we took an IR spectrum and started the monitoring of residue gases by QMS in order to compare the residue molecules and to verify any possible contaminations in the main chamber. We then start the cooling process thanks to the closed-cycle He cryostat.

Deposition

The gas mixtures are pre-mixed in our gasline system introduced in section 1.1.1. We used a leak valve to condense the gas from the stainless steel bottles onto pre-cooled KBr substrate at 14 K, which monitored by Fourier transformed Infra-red spectroscopy (FTIR) and Quadrupole mass spectrometer (QMS) during deposition. The pressure of deposition is fixed to 1×10^{-8} torr that the deposition rate is $4 \times 10^{16} molecules cm^{-2} min^{-1}$. After deposition, we placed the ice mixture at 14 K for 60 minutes and to allow pumping of residue gas, until pressure of the main chamber reduce back to its base pressure to simulate the interstellar environment before irradiation.

Photon Irradiation

The total irradiation time is 270 to 450 minutes depend on experiment configurations; with time intervals varies from 2 to 30 minutes. After each irradiation, we waited for 10 minutes allowing pumping out of the photodesorped gas molecules. During irradiation, the photon flux is monitored by a nickel mesh. After Irradiation, we place the sample for 30 minutes to observe if any thermal reaction was conducted.

Warmup

We use 1 K/min to warmup the substrate to 300 K to demonstrate effects of a new born star nearby an interstellar cloud. During warmup, we record the QMS from 1 to 100 a.m.u. to observe if there are low quantity of higher mass product formed during irradiation.

1.3   Infra-red spectroscopy and the Beer's Law

We used infra-red spectroscopy extensively in chapter 3 and 4, it is a powerful tool in studying molecular interactions during irradiation and warmup. We choose infra-red rather than Ramen spectroscopy because infra-red has lower energy that it would not change the structure of the ice mixture nor breaking any of the bonds. With different vibration modes, the energy absorbed by molecules are quantized. With the energy of absorption bands in infra-red spectrum, we may identify the functional group of the species. To simply classify, molecules can have, from less energetic, translational, rotational and vibrational motions. Generally, vibrational motions can be divided into stretching and bending. Stretching needs more energy than bending. For stretching, there exist Symmetric and Asymmetric stretching, while bending can be divided into In-plane Scissoring, rocking and out of plane Wagging and Twisting (Figure 1.4).

By Beer's Law, we may calculate the column density of the molecule with its functional groups, which are used to plot figures in chapter 3 and 4. Beer Lambert's Law suggest that when light passes through a
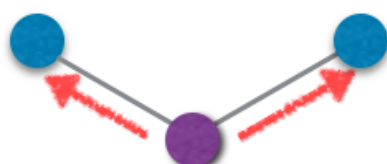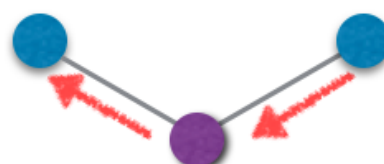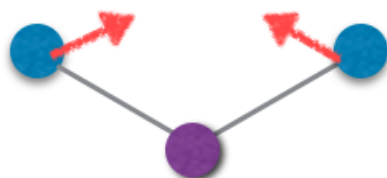
Figure 1.4: Different vibrational modes of a three atom molecule.
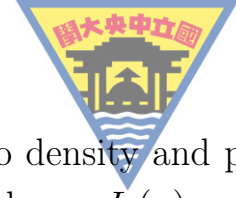
medium, amount of light absorbed is proportional to density and path length of the medium. Assume the known intensity beam $I_0(\nu)$ passes through the medium and beam intensity become $I(\nu)$. The transmittance $T(\nu)$ is defined by equation 1.1.

$$T(\nu) = \frac{I(\nu)}{I_0(\nu)} \tag{1.1}$$

Also, the absorbance $a(\nu)$ is defined by equation 1.2.

$$a(\nu) = -\ln T(\nu) = -\ln \frac{I(\nu)}{I_0(\nu)} = nl\sigma(\nu) \tag{1.2}$$

where n is number density (molecules/cm^3), l is the path length (cm), $\sigma(\nu)$ is the cross-section (cm^2/molecule) of corresponding frequency ν. This equation is known as Lambert Beer's Law.

As the ice mixture in our thesis are at 14K, the peaks of absorbance are often a broadband due to coupling between neighbor molecules. Therefore, we can integrate the whole band of the peak equation 1.2 with respect to frequency and use the absorbance strength (A value) in literatures to calculate the column densities N of the ices by equation 1.3.

$$N = \frac{\int a(\nu)\mathrm{d}\nu}{A(\nu)} \tag{1.3}$$

where N is the column density (molecule cm^{-2}), $A(\nu)$ is the absorbance strength (cm molecule^{-1}).

1.4 Reaction Rate Laws

In this section, we will introduce rate reaction of a consecutive reaction and the concept of pseudo first order which we used to fit our reaction product against irradiation time. The rate of a chemical reaction is the relation between change in concentration of a substance per unit of time. i.e. For a balanced chemical reaction, A $\rightarrow$ 2B, the rate of reaction is $-\frac{\Delta[A]}{\Delta t}$. The formation rate of B is 2 times destruction rate of A.

To determine the order of a reaction, we can only determine it experimentally. For a zero order reaction, the rate is not depending on any reactant that it is a constant. The rate $= -\frac{\Delta[R]}{\Delta t} = k[R]^0$. By calculus, $[R]_0 - [R]_t = kt$.

For a first order reaction, rate $= -\frac{\Delta[R]}{\Delta t} = k[R]$. By calculus, $\ln[R]_t = -kt + \ln[R]_0$.

For a second order reaction, rate $= -\frac{\Delta[R]}{\Delta t} = k[R]^2$. By calculus, $\frac{1}{[R]_t} - \frac{1}{[R]_0} = kt$.

Hence, if we get a straight line in a time versus concentration plot ,it is a zeroth order reaction, similarly, in first order reactions, we get proportional relationships in time versus $\ln[R]$.

In a reaction with one reactant in excess, the rate of reaction is called pseudo first order reaction where pseudo means pretended. For A+B $\rightarrow$ C, rate $= k[A][B]$. As $[B]_0 \gg [A]_0$, change of $[B]$ is negligible that $[B] \sim [B]_0$. Therefore, $[B]$ is assumed to be a constant and included in the rate constant k.

For a consecutive reaction equation, which we used to fit our data points, where A $\rightarrow$ B $\rightarrow$ C that the produced product will not convert back as reactant. A simple example is radioactive decay. At $t = 0$, $[A] = [A]_0$, $[B] = 0$, $[C] = 0$ and at all times, $[A] + [B] + [C] = [A]_0$. The rate equations are as follows:

$$-\frac{\Delta[A]}{\Delta t} = k_1[A] \tag{1.4}$$

$$-\frac{\Delta[B]}{\Delta t} = k_1[A] - k_2[B] \tag{1.5}$$

$$-\frac{\Delta[C]}{\Delta t} = k_2[B] \tag{1.6}$$

By equation 1.4, we get

$$[A] = [A]_0 e^{-k_1 t} \tag{1.7}$$

By substituting equation 1.7 into equation 1.5, we get

$$-\frac{\Delta[B]}{\Delta t} + k_2[B] = k_1[A]_0 e^{-k_1 t} \tag{1.8}$$

After solving the differential equation 1.8 , we get

$$[B] = \frac{k_1}{k_2 - k_1}(e^{-k_1 t} - e^{-k_2 t})[A]_0 \qquad (1.9)$$

Finally, since $[C] = [A]_0 - [B] - [A]$, by equation 1.7 and 1.9, we get

$$[C] = \left(1 + \frac{k_1 e^{-k_2 t} - k_2 e^{-k_1 t}}{k_2 - k_1}\right)[A]_0 \qquad (1.10)$$

2. Results and Discussions

According to the New Horizons team [?], CH_4 from Pluto may accumulate by cold-trapping, onto the surface of Charon. The amount of CH_4 varies along the surface of Charon because it depends on the length of time the temperature is below 25 K which in turns depends on diurnal motion and thermal inertia of Charon. With an axis tilted by 112 degrees from the ecliptic, higher concentration of CH_4 will be accumulated at the pole (see chapter ?? for details). In this chapter, we will investigate the following by infra-red spectroscopy: 1. The photo products produced by different concentration ratios of methane to ammonia, 2. the photo products produced by different photo sources (i.e. EUV and VUV) 3. the reaction mechanisms of each main products and 4. the functional group of tholin formed by irradiation of VUV, EUV on different configurations of CH_4+NH_3 ice mixtures (the result is compared with the residues on Titan produced by Imanaka et al. [?]).

2.1 The infra-red spectrums and peaks identification

We scanned the IR spectrum before and after deposition and plotted the plot the corresponding absorbance of the ice mixtures. Figure 2.1 is a plot of the absorbance of the CH_4+NH_3 ice mixtures in different concentration ratios: 1:20, 1:10, 1:5 and 3:2 (arrangedfrom top to bottom). We labelled the peaks used in column density calculation by dotted lines in the graph. Main products we have detected are C_2H_6, CN^- and C_3H_8. The peak positions for substance identification are listed in Table 2.1. After identification of the products, we will look into each main products individually.

To calculate the column density, we integrate the area under graph
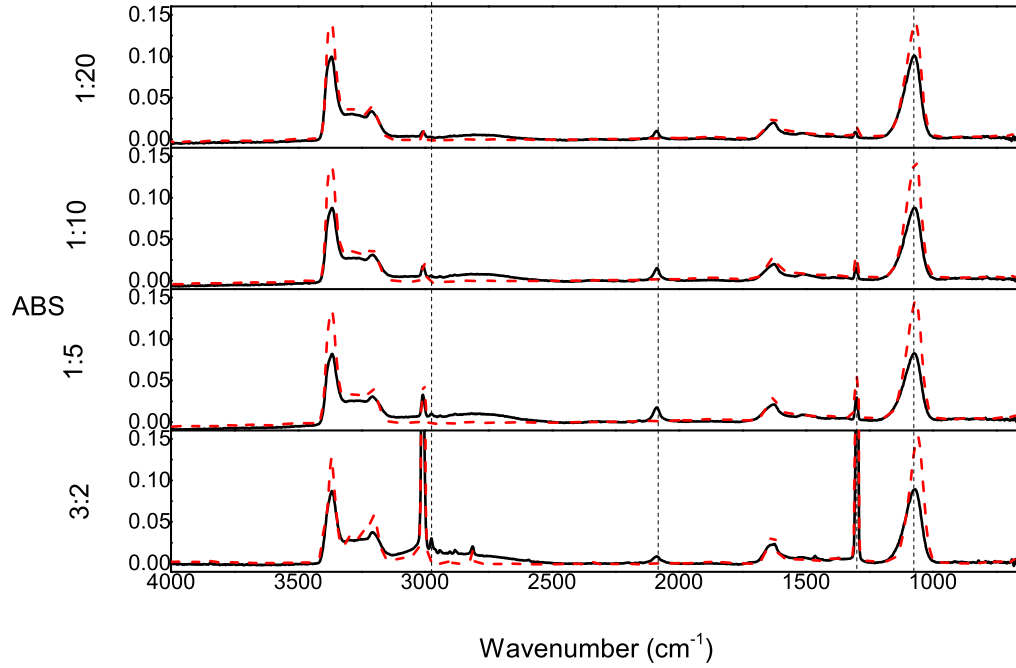
Figure 2.1: The the infra-red spectrum of $CH_4 + NH_3$ ice mixtures before irradiation (dashed) and VUV irradiated ice mixtures provided by MDHL.

Table 2.1: The peak positions of identified substances after irradiation in different configurations of ice mixtures.

Literture assignments		CH$_4$+NH$_3$ ratio (MDHL)				
Wavenumber	Carrier	1:5	1:10	1:20	3:2	Ref.
(cm^{-1})		(cm^{-1})	(cm^{-1})	(cm^{-1})	(cm^{-1})	
3375	ν_3 (NH$_3$)	3366	3366	3369	3367	1
3290	$2\nu_4$ (NH$_3$)	-	-	-	-	1
3210	ν_1 (NH$_3$)	3207	3208	3210	3205	1
3011	ν_3 (CH$_4$)	-	-	-	-	2
2972	ν_{10} (C$_2$H$_6$)	2975	-	-	2975	3
2960	C$_3$H$_8$	-	-	-	2960	7
2941	$\nu_8 + \nu_1 1$ (C$_2$H$_6$)	2940	-	-	2940	3
2904	ν_1 (CH$_4$)	2901	-	-	2901	5
2879	ν_5 (C$_2$H$_6$)	2882	2883	-	2882	3
2814	$\nu_2 + \nu_4$ (CH$_4$)	-	-	-	2815	5
2083	ν (CN$^-$)	2088	2087	2088	2088	2
1625	ν_4 (NH$_3$)	1625	1625	1626	1631	1
1514	δ (NH$_2$)	1509	1507	1505	1511	6
1465-1440	deform CH$_2$ scissor	1461	-	-	1463	3,4
1390-1370	CH$_3$ sym deform	1394	1394	1394	1372	4
1298	ν_4 (CH$_4$)	1301	1302	1305	1299	2
1075	ν_2 (NH$_3$)	1073	1072	1072	1072	1
820	$\nu_1 2$ (C$_2$H$_6$)	-	-	-	820	3

Reference: 1. Bossa et al. 2008 [?] 2. Moore and Hudson 2003 [?] 3. Kim et al. 2010 [?] 4. Socrates 2001 [?] 5. Bennet and Kaiser 2007 [?] 6. Zheng et al. 2008 [?] 7. Hudson and Moore 2004 [?]

and divided by the absorption strength presented in table 3.2. We aware that there is an average error in absorption strengths of no more than 10 % when the pure ice is diluted in N_2 and H_2O [?]. In our case, absorption strengths changes after CH_4 and NH_3 are mixed. For example, according to d' Hendecourt and Allamandola [?], the band of NH_3 located at 1070 cm^{-1} would not change much (from 1.1×10^{-17} to 1.2×10^{-17}) when excess water is added to pure NH_3. For the case of CN^-, we know that CN^- has a bond order $=3$ from its molecular orbitals. CN^- which is different from CN (bond order 2.5). CN stretching is very sensitive to the matrix environment. It can change by factor of 2 in amino acetonitrile and H_2O (1:3) [?]. However, CN is not inspected in this chapter. Therefore, we are justified to use the same absorption strength throughout our discussion to estimate the column density of each species and how the absorption area changes with concentration ratios of ice mixtures and photon energy. Here, we adopt the absorption strengths stated in Table 2.2

Table 2.2: The strength of absorbance adopted in this thesis measured in literatures of pure ice samples

Wavenumber (cm^{-1})	Assignment	Vibration	FWHM	A value ($\times 10^{-17}$)	Reference
2976	C_2H_6	$-CH_3$	-	1.05	2
2960	C_3H_8	$-CH_2-$	-	2.58	2
2086	CN^-	CN	-	1.8	3
1297	CH_4	CH deformation	8	0.61	1
1070	NH_3	"umbrella mode"	68	1.7	1

Reference: 1. d'Hendecourt and Allamandola (1986)[?] 2. Moore and Hudson (1998)[?] 3. Noble et al. (2013) [?]

2.2   Reaction mechanisms

2.2.1 C_2H_6

The assignment of C_2H_6 is confirmed by several bands listed in table 2.1. Figure 2.2 is a zoomed view of figure 2.1. The absorption peak located at 2075 cm^{-1} corresponds to the strongest vibration of C_2H_6. The formation of C_2H_6 in astrophysical environment is mainly through a combination with 2 CH_3 radicals [?]:

$$CH_4 + hv \rightarrow CH_3 \tag{2.1}$$

Figure 2.2: The the infra-red spectrum of CH_4 + NH_3 ice mixtures of C_2H_6 and C_3H_8 before irradiation (dashed) and VUV irradiated ice mixtures provided by MDHL.

$$2CH_3 \rightarrow C_2H_6 \tag{2.2}$$

The energy required to produce 1 CH_3 radical from CH_4 is 4.42 eV. Recombination of 2 CH_3 radicals to form C_2H_6 releases 3.74 eV. The process in 2.2 is a no-barrier exothermic process. Note that C_2H_6 is not detected in CH_4 to NH_3=1:20 ice mixtures. Figure 2.3 shows the temporal formation column density of C_2H_6 in different configurations of irradiated ice mixtures. As the formation only depends on CH_4, we may use first order kinetics equation to fit the column density versus photon dose.

$$[A] = [A]_0(1 - e^{-k_1 t}) \tag{2.3}$$

The fitting results are shown in table 2.3.

Table 2.3: The fitting results of C_2H_6 by $[C_2H_6]=[C_2H_6](1 - e^{-k_1 t})$

Ratio of CH_4+NH_3	A (x10^{15} molecules cm^{-2})	k (x10^{-17} photon^{-1})
1:10	2.90 ± 1.25	0.92 ± 0.15
1:5	4.16 ± 0.28	2.28 ± 0.28
3:2	19.2 ± 0.15	5.28 ± 0.25
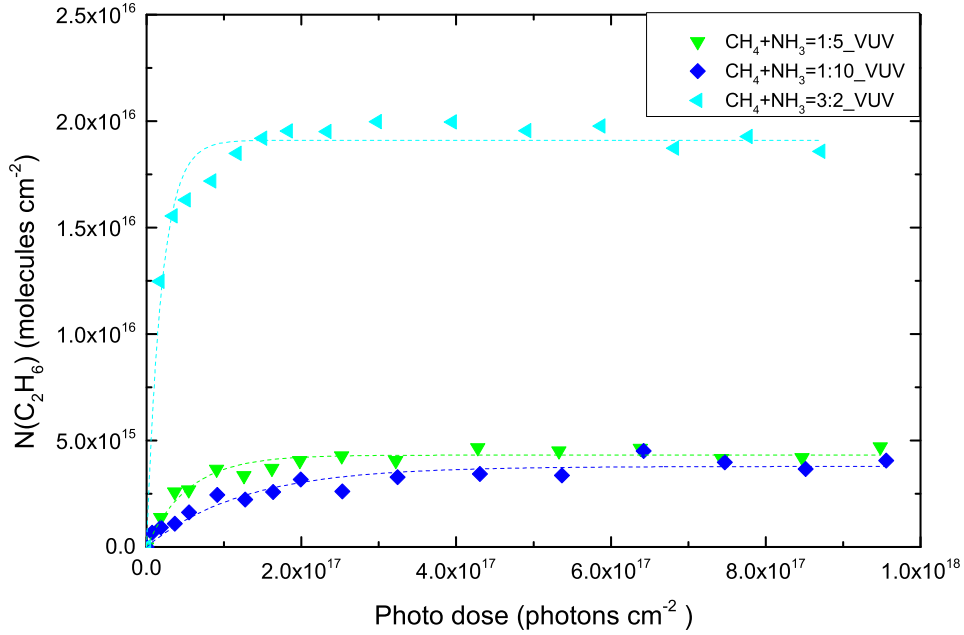
Figure 2.3: The column density of C2H6 during CH4 + NH3 ice mixtures irradiated by MDHL.

From table 2.3, the production rate is nearly proportional to the initial CH_4 concentration.

2.2.2 C_3H_8

The peak positioned at 2960 cm^{-1} belongs to –CH$_2$- so we assigned that as C_3H_8, as the shortest carbon chain. The signal to noise ratio in $CH_4+NH_3 = 1:10$ is poor that we can not quantize the amount of C_3H_8 (figure 2.2).

It is a secondary product formed by a combination of either C_2H_6 + CH_2 (equation 2.4)or C_2H_4 + CH_4 (equation 2.5).

$$C_2H_6 + CH_2 \rightarrow C_3H_8 \tag{2.4}$$

$$C_2H_4 + CH_4 \rightarrow C_3H_8 \tag{2.5}$$

By modern peak fitting method, we deconvoluted the overlapped C_2H_6 and C_3H_8 into two gaussians.

2.2.3   CN$^-$

From infra-red absorption spectrum (figure 2.4) and their positions, we assigned the peak 2086 cm^{-1} to CN$^-$ but not a combination of HCN

17
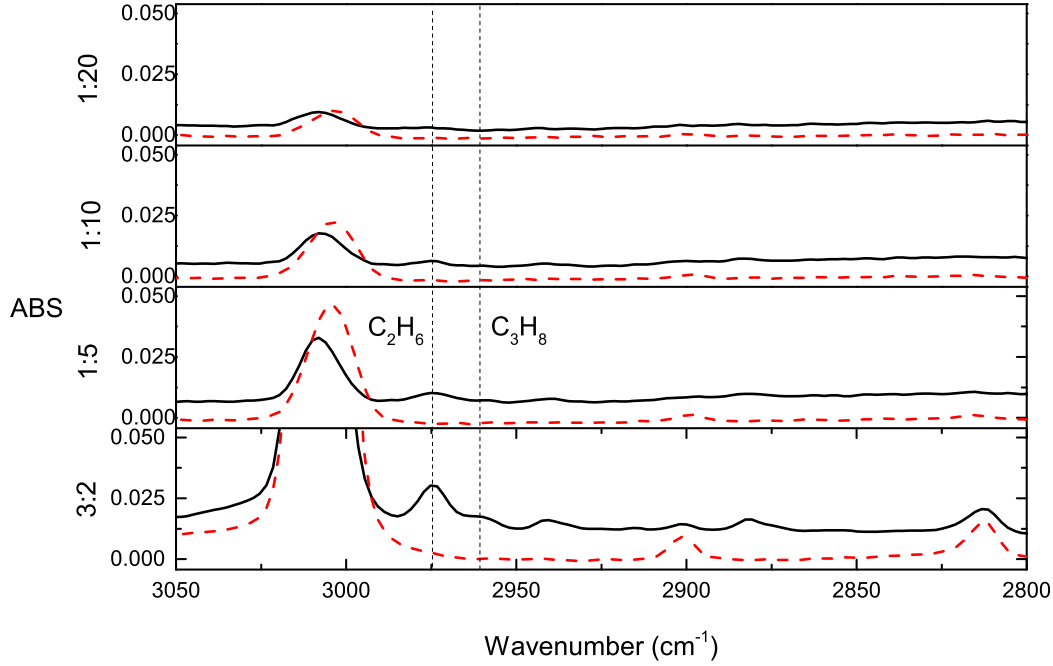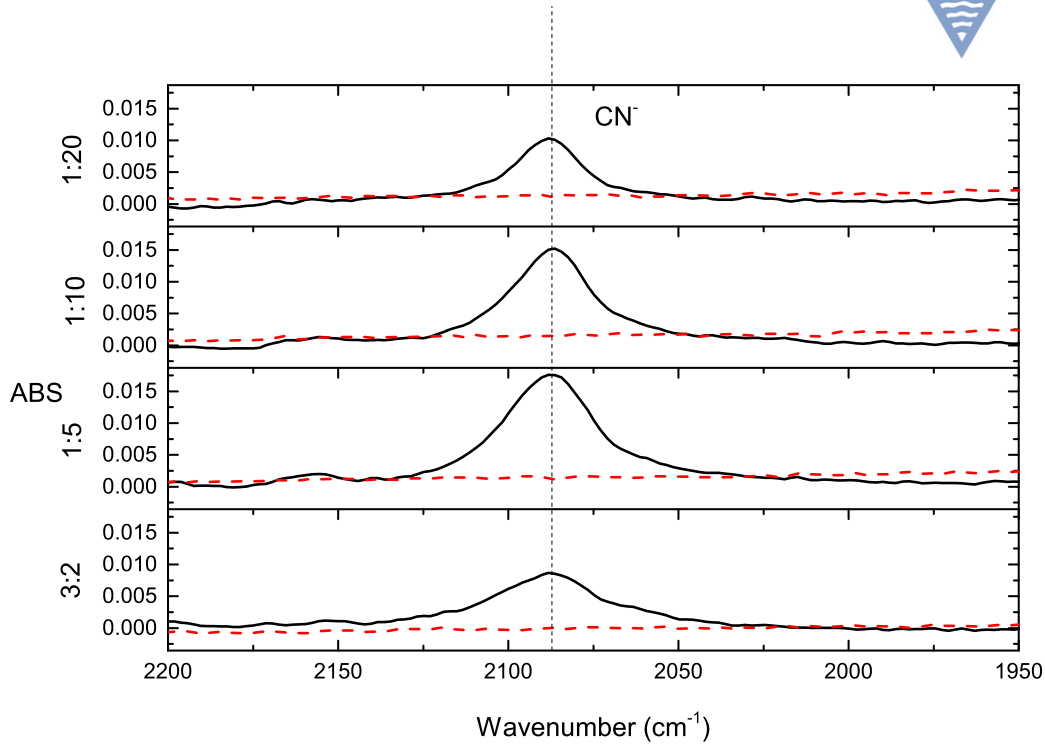
Figure 2.4: The the infra-red spectrum of $CH_4 + NH_3$ ice mixtures of C_2H_6 and C_3H_8 before irradiation (dashed) and VUV irradiated ice mixtures provided by MDHL.

and CN^-. The assignment is based on a absence in CN bending mode at 848 cm^{-1}. In the case $CH_4 + NH_3 = 3:2$, we may observe a peak located at 820 cm^{-1}, which is with a FWHM half of HCN and it is eliminated at 50 K during the warm-up phase. Since 50 K is the desorbing temperature of C_2H_6 and the peak position is the close to v12 mode of C_2H_6, we believe that the 820 cm^{-1} peak is contributed by C_2H_6. Therefore, we may assign our peak located at 2086 cm^{-1} as purely CN^-.

The formation mechanism of CN^- at low temperature was first suggested by Kim and Kaiser [?] to be two step reaction mechanism with methylamine as intermediate. CH_4 and NH_3 irradiated by photon to become CH_3 and NH_2 radical (figure 2.5, followed by propagation and recombination of radicals becoming CH_3NH_2 and dehydrogenation and acid-base reaction to form CN^-. Although Kim and Kaiser [?] used 1.5 keV electron as energy source to simulate the cosmic ray induced photochemistry, this formation mechanism also applies in our photon

Figure 2.5: The formation mechanism of CN^- proposed by Kim and Kaiser(2011).

irradiation experiments because we can also detect the methylamine during our warm-up phase. The ion fragment with m/z=31 is assigned as $CH_3NH_2^+$ and detectable in all ratios of our CH_4+NH_3 experiments (figure 2.6).

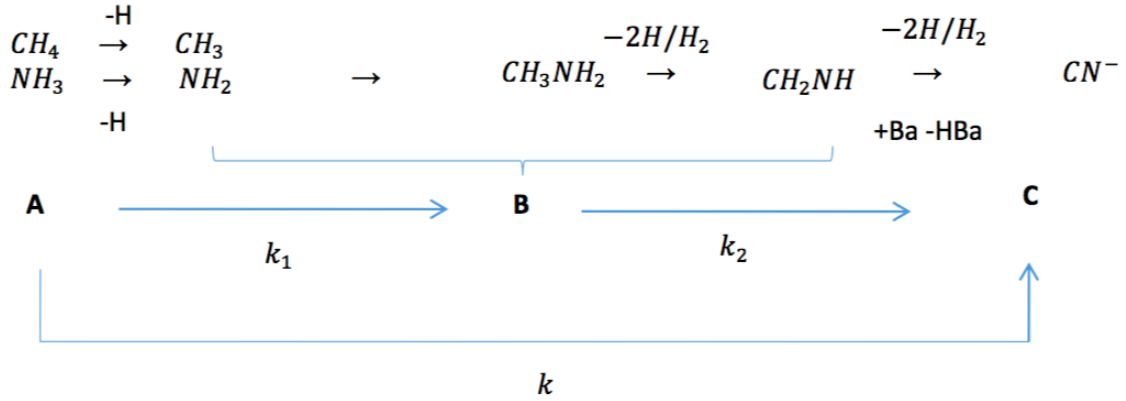By the deviation performed in section 1.4, we have a rate equation for consecutive reactions 1.10. With one of the reactant larger than another, we applied the pseudo first order assumption. With equation 1.10, we fitted the formation of CN^- (figure 2.7)and found that one of the rate constant is always larger than the other in all of the ratios. The fitting results are averaged by more than two experiments and are shown in table 2.6.The results of Kim and Kaiser is also listed into the table, they could observe a two-step reaction mechanism in production of CN^- in CH_4+NH_3 (3:1) experiments with electron current 0.1 μA. However, when they increased the electron flux to 1 μA for irradiation $C_nH_{2n+2(n=1-6)}$ and NH_3 ice mixtures, they also observed a one-step reaction mechanism.

Table 2.4: The fitting results of CN^- by equation 1.10

Ratio of CH_4+NH_3	A (x10^{16} molecules cm^{-2})	k_1 (x10^{-18} photon^{-1})	k_2 (photon^{-1})	
1:20	4.75 ± 0.40	0.70 ± 0.09	>1	
1:10	4.51 ± 0.18	1.33 ± 0.13	>1	A
1:5	4.61 ± 0.18	1.93 ± 0.19	>1	
3:2	2.24 ± 0.03	8.21 ± 0.70	>1	

represents the amount of CN^- we may obtain when irradiated the ice for infinitely long.

19
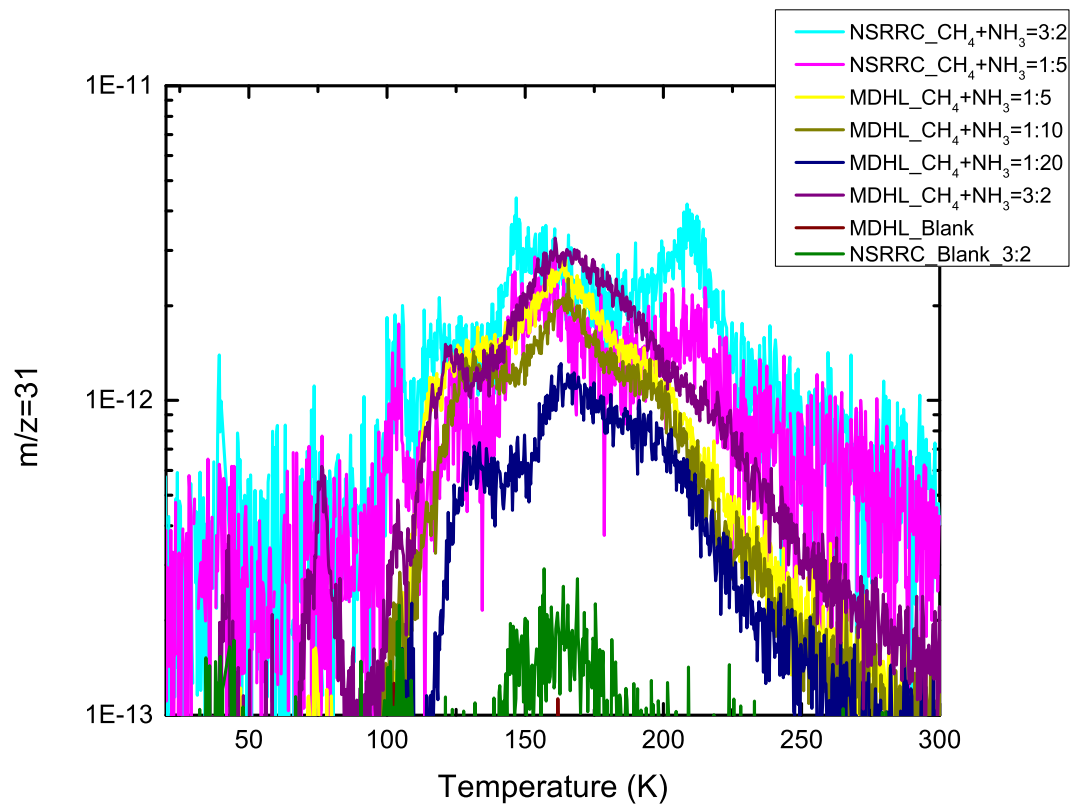
Figure 2.6: The m/z=31 detected by QMS during warm-up with heating rate 1 K/min in different configurations of ice mixtures.
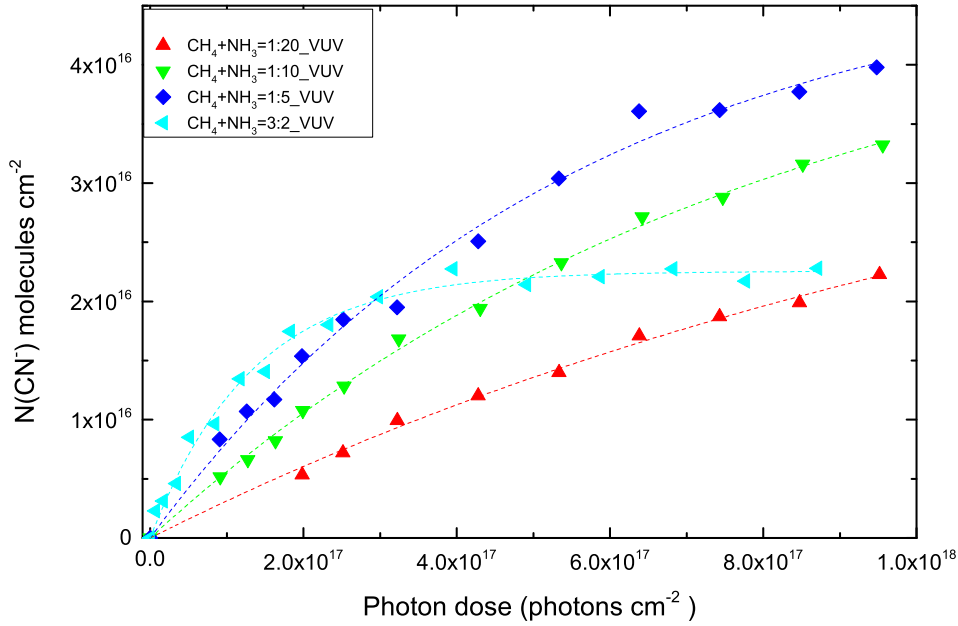
Figure 2.7: The column density of CN^- accumulated when different configurations of CH_4 + NH_3 ice mixtures are irradiated by VUV photons provided by MDHL. The dotted lines are fits of column densities by equation 1.10.

2.3 The Concentration Effect in formation of Cyanide ions and Ethane

2.3.1 Cyanide ion

From table 2.6, we may observe that the rate k_1 is nearly proportional to the concentration of CH_4. As CH_4 to NH_3 ratio increases, more CH_4 are involved in CH_3 radical formation, thus there are more CH_3 radicals to produce CH_3NH_2 intermediates.

In CH_4 to NH_3 =3:2 ice mixtures, A is about half of that of the other ratios. The reduction is mainly because NH_2 (forming CH_3NH_2) has a competing relationship with CH_2, CH_3 and C_2H_4 radicals (forming C_2H_6 and C_3H_8). This competition supresses the production of intermediate CH_3NH_2, thus the formation of CN^-. Therefore, the yield of CN^- is the least in CH_4 to NH_3 ice mixture with ratio 3:2 while the yield of C_2H_6 is the greatest in the mixture with the same ratio(table 2.6), (table 2.3)

Figure 2.8: The column density of CN^- divided by initial CH_4 accumulated when different configurations of $CH_4 + NH_3$ ice mixtures are irradiated by VUV photons provided by MDHL.

Considering the normalized CN^- with respect to the initial CH_4(figure 2.8), the formation of CN^- is more efficient in low CH_4 concentration ice mixtures. At low CH_4 concentration, there are excess NH_3 which can aggregate mobile CH_3 radicals, preventing meeting another CH_3 radical or C_2H_4. Therefore the production of C_2H_6 is greatly suppressed and more CN^- will be produced.

2.3.2   Ethane

Considering the case of ratio of CN^- divided by C_2H_6,the formation of CN^- in ice mixtures with diluted CH_4 has more CN^- formed then C_2H_6. It is because ice mixtures with with higher concentrations in CH_4 is more effective for one CH_3 radical to combine with another CH_3 radical. On the contrast, CH_3 radicals formed in the ice mixtures with diluted CH_4 concentrations are aggregated by NH_3. Therefore, CN^- is less efficient to form in ice mixtures with excess NH_3.

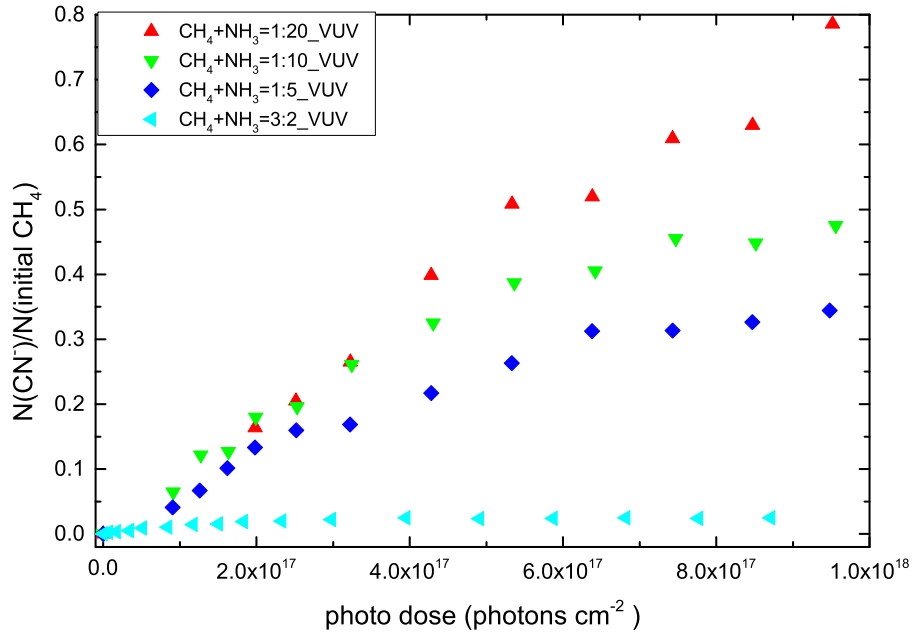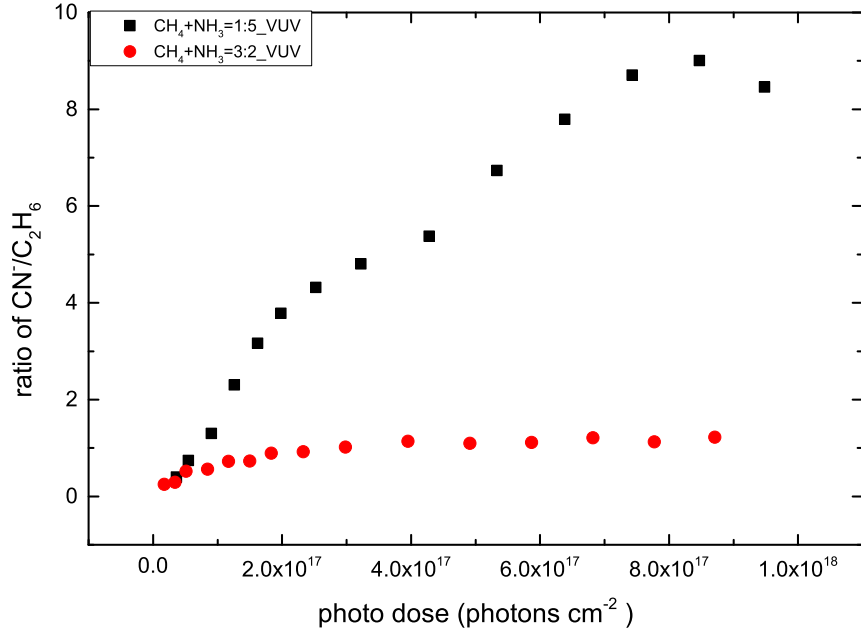Figure 2.9: The column density of CN^- divided by C_2H_6 accumulated when different configurations of $CH_4 + NH_3$ ice mixtures are irradiated by VUV photons provided by MDHL.

Figure 2.10: The column density of C_3H_8 divided by C_2H_6 accumulated when different configurations of $CH_4 + NH_3$ ice mixtures are irradiated by VUV photons provided by MDHL.
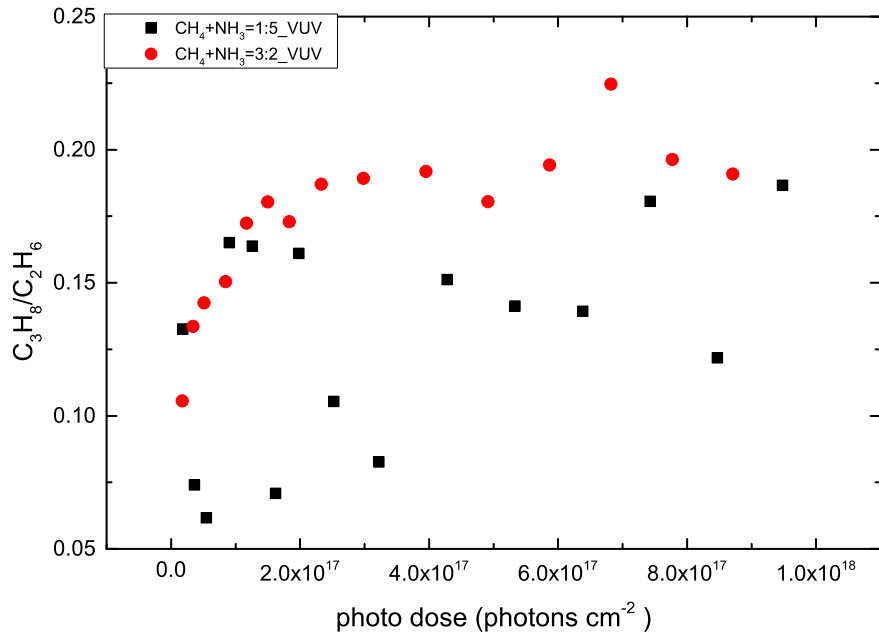
2.3.3   Propane

C_3H_8 forms based on to the C_2H_6 2.10 is the plot with column densities of C_2H_6 divided by C_3H_8. We may see that the ratio in CH_4+NH_3 =1:5 experiment is around 6 where CH_4+NH_3 =3:2 is around 3. This shows that the amount of C_3H_8 in CH_4+NH_3 =3:2 experiment is higher. It is rather difficult for C_3H_8 to form in CH_4+NH_3 = 1:5 experiments because NH_3 aggregated them. The formation of C_3H_8 in CH4+NH3 =1:5 and 3:2 experiments has given a reasonable explanation about why C_2H_6 formation is most efficient in CH_4+NH_3 =1:10 experiments.

2.4   Photon Energy Effect - EUV and VUV

According to Blanksby and Ellison [?], the dissociation energy for CH_4, becoming CH_3, CH_2 CH and C are 4.55, 4.79, 4.39 and 3.51 eV respectively at 298 K. Whereas dissociation energy for NH_3, becoming NH_2 is 4.67 eV at 298 K.

Considering our MDHL with average energy of 9.27 eV, all of the above fragments may exist either in the form of radicals or combined with other radicals to form heavier molecules in our ice mixtures. Although Increasing the photon energy does not create new fragmentation pathway, the choice of fragmentation pathways depends on photon energy.

Several gaseous state measurements also support this statement. First, Gans et al. (2011) [?] changed VUV photon wavelengths from 121.6 nm to 118.2 nm to dissociate the CH_4 molecules and ionize the fragments with the corresponding photon energy. Changing the output of the pulsed laser from 121.6 to 118.1 nm significantly changed the ratio of CH_3^+ and CH_2^+, produced from fragmentation, from 1: 1 to 1:2. This slight change of photon energy, from 10.2 eV to 10.4 eV has a significant change in the ratio between different pathways.

Second, an EUV fragmentation experiment done by Tsai et al. [?] used 30.4 nm to photo-dissociate CH_4 and tested it by timeĂŞ-ofĂŞ-flight mass spectrometer yields CH_3^+: CH_2^+: CH^+: C^+ = 1 :0.32: 0.118: 0.0237 (Tsai 1980). Consider the ratios of CH_3 to CH_2 radicals, it is around 3 to 1, which is in contrast to the experiment results of Gans
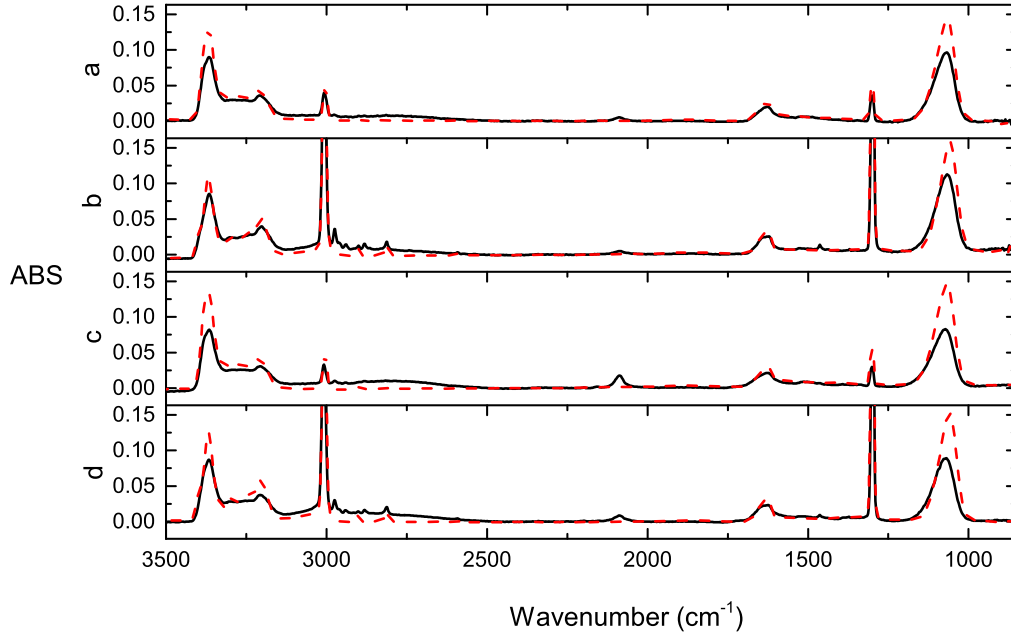
Figure 2.11: The the infra-red spectrum of CH_4 + NH_3 ice mixtures before irradiation (dashed) and VUV and EUV (solid) irradiated ice mixtures provided by MDHL. (a) and (b) are EUV irradiated CH_4+NH_3 = 1:5 and 3:2 ice mixtures respectively, and (c) and (d) are VUV irradiated CH_4+NH_3 = 1:5 and 3:2 ice mixtures respectively.

et al. (2011)[?]. Although both of them are gaseous state experimental results, it is uncertain that if increasing photon energy can produce more CH_2 radicals.

Thirdly, a group varies ratios of CH_4 + NH_3 mixtures and irradiate with far UV irradiation at 134 nm [?]. However, this group only used gas chromatography to analyse the final products and their reaction is carried in gas phase in room temperature. We aware that the VUV absorption spectra of CH_4 in solid phases is different from gaseous phases [?], so the exact photo dissociation fragmentation ratios by EUV nor VUV irradiations in astronomical environments are still unknown. It is worthwhile for us to perform the experiment by EUV irradiation to see if EUV irradiation can generate any new products on the surface of Charon, or any difference in yield. Despite the photon energy of our MDHL is enough to dissociate both the CH_4 and NH_3 molecules, we further increase photon energy to He II 30.4 nm to examine the differences in photo-products.

Table 2.5 shows the identified peaks of CH_4+NH_3 ice mixtures irradiated by VUV and EUV (30.4 nm) irradiated in IR spectra (figure 2.11).

Table 2.5: The peak positions of identified substances after VUV and EUV irradiations in different configurations of ice mixtures.

Literture assignments		CH$_4$+NH$_3$ ratio (MDHL)		CH$_4$+NH$_3$ ratio (30.4 nm)		
Wavenumber (cm^{-1})	Carrier	1:5 (cm^{-1})	3:2 (cm^{-1})	1:5 (cm^{-1})	3:2 (cm^{-1})	Ref.
3375	ν_3 (NH$_3$)	3366	3367	3368	3368	1
3290	$2\nu_4$ (NH$_3$)	-	-	-	-	1
3210	ν_1 (NH$_3$)	3207	3205	3209	3205	1
3011	ν_3 (CH$_4$)	-	-	-	-	2
2972	ν_{10} (C$_2$H$_6$)	2975	2975 2977	2976		3
2960	C$_3$H$_8$	-	2960	-	2960	7
2941	$\nu_8 + \nu_1 1$ (C$_2$H$_6$)	2940	2940	-	2942	3
2904	ν_1 (CH$_4$)	2901	2901	2901	2901	5
2879	ν_5 (C$_2$H$_6$)	2882	2882	-	2884	3
2814	$\nu_2 + \nu_4$ (CH$_4$)	-	2815	-	2813	5
2083	ν (CN$^-$)	2088	2088	2090	2089	2
1625	ν_4 (NH$_3$)	1625	1631	1627	1631	1
1514	δ (NH$_2$)	1509	1511	1509	1511	6
1465-1440	deform CH$_2$ scissor	1461	1463	-	1465	3,4
1390-1370	CH$_3$ sym deform	1394	1372	-	1372	4
1298	ν_4 (CH$_4$)	1301	1299	1303	1301	2
1075	ν_2 (NH$_3$)	1073	1072	1070	1068	1
820	$\nu_1 2$ (C$_2$H$_6$)	-	820	-	-	3

Reference: 1. Bossa et al. 2008 [?] 2. Moore and Hudson 2003 [?] 3. Kim et al. 2010 [?] 4. Socrates 2001 [?] 5. Bennet and Kaiser 2007 [?] 6. Zheng et al. 2008 [?] 7. Hudson and Moore 2004 [?]

Considering the formation mechanisms of C$_2$H$_6$ and C$_3$H$_8$, equation (2.2 and 2.4), when MDHL VUV irradiation is replaced by He II 30.4 nm monochromatic light, the ratio of C$_2$H$_6$ to C$_3$H$_8$ in CH$_4$ to NH$_3$ = 3:2 ice mixtures irradiated by VUV irradiation is lower under EUV irradiation than that under EUV provided by NSRRC (figure 2.12). There are two possible explanations. First, different photon energies flavour different CH$_4$ fragmentation pathway and less C$_3$H$_8$ is produced with EUV photons. Second, the efficiency of CH$_4$ fragmentation is greatly reduced under EUV irradiation and the density of CH$_3$ radicals are much lower than that in the case of VUV irradiation provided by the MDHL. We lengthen the time of EUV irradiation on our ice mixtures until the total number of destructed CH$_4$ is similar to that in VUV irradiation experiments done with MDHL. The averages of ratios of C$_2$H$_6$:C$_3$H$_8$ of the last 7 irradiations before terminating irradiations are 3.53 in VUV and
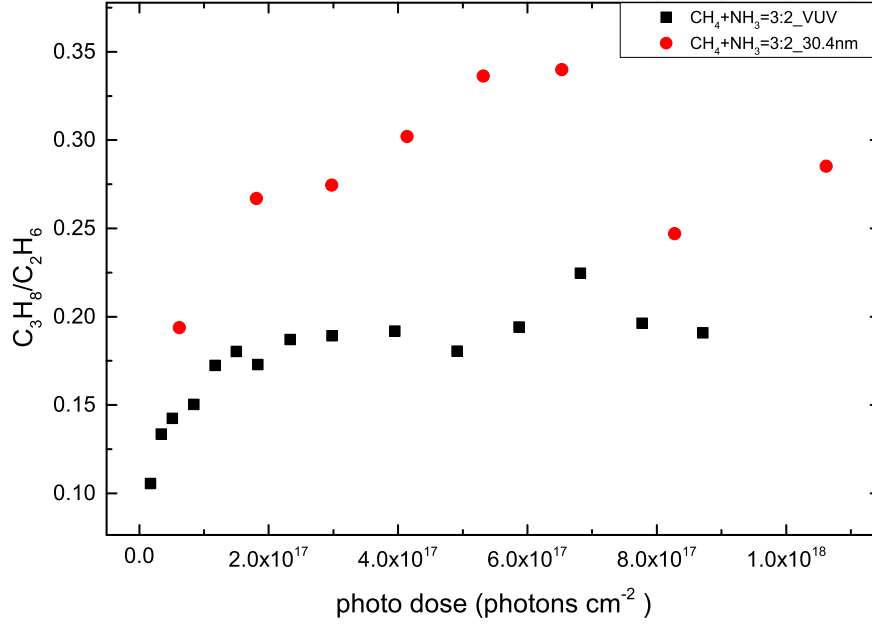
Figure 2.12: The column density of C_3H_8 divided by C_2H_6 accumulated when different configurations of $CH_4 + NH_3$ ice mixtures are irradiated by VUV and EUV photons

3.66 in EUV. The result supports the latter explanation. From figure 2.13, The reduction of CH_4 is 6.06$\pm$ times slower in EUV experiments than VUV experiments while the reduction of NH_3 is 3.19$\pm$0.12 times slower. Therefore, the destruction cross-section of CH_4 and NH_3 ice has a 6.06$\pm$0.07 and 3.19$\pm$0.12 times lower in 30.4 nm than in 121.6 nm.

Figure 2.12 shows the column densities of C_2H_6 divided by C_3H_8 after $CH_4 + NH_3$ =3:2 ice mixtures are irradiated by VUV irradiation and He II monochromatic light.

From 2.12, we may observe that more C_3H_8 is produced by 30.4nm photons than by VUV photons. Recall the formation mechanism of C_3H_8 (equation 2.5), CH_2 and C_2H_4 radicals are esscential in producing C_3H_8. This increase production in C_3H_8 may be caused by the increase in CH_2 radicals during fragmentation of CH_4. This result is similar to the findings of Gans et al. (2011)[?], the ratio of CH_2 radicals increases from 0.3 to 0.48 when photon energy increases from 121.6 nm to 118.2 nm in their pulsed laser experiments.

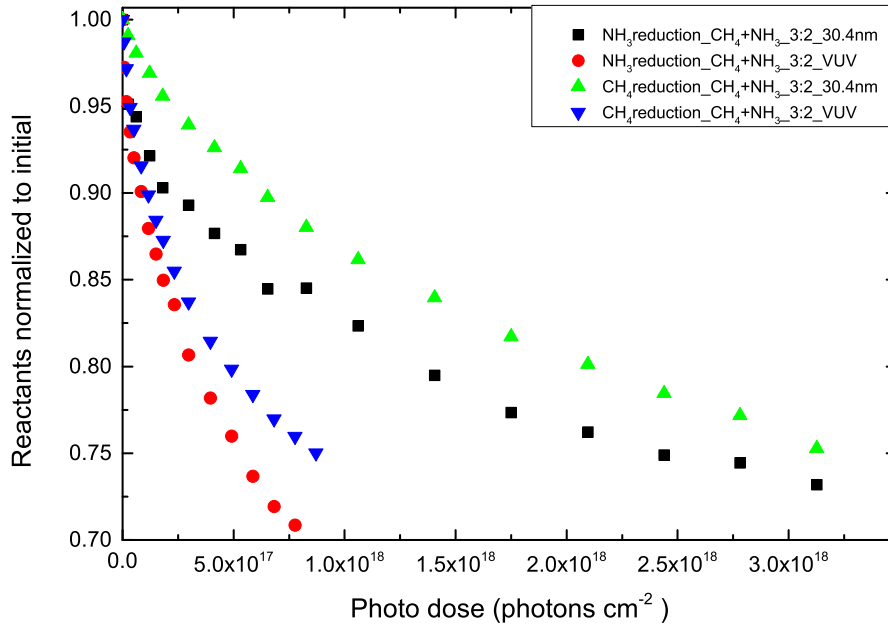Apart from C_2H_6 and C_3H_8, are there any difference in CN^- pro-

Figure 2.13: The normalized reduction of CH_4 and NH_3 in $CH_4 + NH_3$ ice mixtures irradiated by VUV and EUV photons

duction? Figure 2.14 shows the accumulated column densities of CN^- generated by irradiation of CH_4+NH_3 ice mixtures by MDHL and 30.4 nm monochromatic light. The fitting results are shown in Table 3.6. The rate constants forming CN^- is 3.06 to 4.13 times larger in CH_4+NH_3 = 1:5 and 3:2 irradiated by MDHL than irradiated by 30.4 nm monochromatic light respectively. From figure 2.13, the CH_4 reduction in NSRRC is 6.06±0.07 times slower. With the rate constants of CN^- only 3.06 to 4.13 times smaller, the 6 times slower in CH_4 reduction and 3 times slower in CN^- formation give rise to a similarity of reduced NH_3 destruction cross-section and reduced rate in CN^- production in EUV irradiation experiments. Therefore, we may conclude that the reduction in CN^- formation rate by 30.4nm EUV irradiation is mainly due to the decreased NH_3 destruction cross-sections.

2.5 Residues

The residues we studied are the accumulated residues onto the substrate. We do not understand are there any interaction between residues and the ice mixtures. However, we may know what is the change of
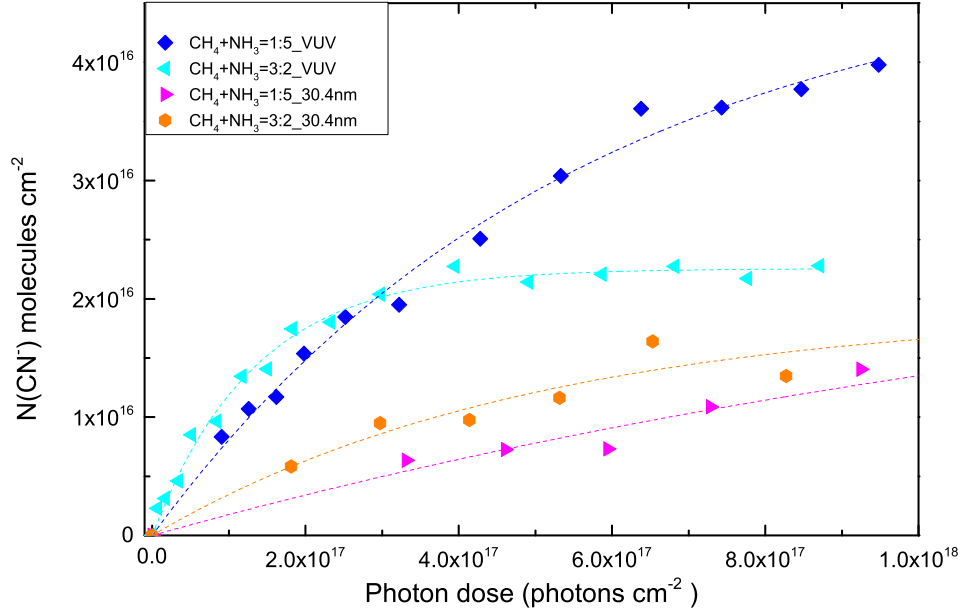
Figure 2.14: The column densities of CN$^-$ generated by irradiation of CH$_4$+NH$_3$ ice mixtures by MDHL and 30.4 nm monochromatic light.

Table 2.6: The fitting results of CN$^-$ by equation 1.10

Light source	Ratio of CH$_4$+NH$_3$	A (x10^{16} molecules cm^{-2})	k$_1$ (x10^{-18} photon^{-1})	k$_2$ (photon^{-1})
VUV	1:5	4.61 ± 0.18	1.93 ± 0.19	>1
MDHL	3:2	2.24 ± 0.03	8.21 ± 0.70	>1
EUV	1:5	2.89 ± 1.29	0.63 ± 0.37	>1
30.4nm	3:2	2.24 ± 0.03	1.92 ± 1.99	>1

Fitting result of figure 2.14 with pseudo first order equation [CN$^-$]=$A(1 - e^{-kx})$. These fitting results of MDHL experiments are an average of at least 2 experiments with the same circumstances. In the expression, A represents the column density when x, the photon dose, becomes infinitely large and k is the rate constant.

residues when we change the ratio of the CH_4+NH_3 from CH_4 dominating to NH_3 dominating. Figure 2.15 is a comparison of CH_4+NH_3 = 3:2 after VUV experiments, residues accumulated after EUV exposure of $CH_4 + NH_3$ = 3:2 ice mixtures and the plasma experiment done by Imanaka et al. (2004)[?]. The residues in ammonia dominated ice mixtures cannot be detected after consecutive experiments. There are no differences between EUV accumulated residues and VUV accumulated residues in CH_4+NH_3 = 3:2 ice mixtues. The main differences between plasma experiments of N_2+CH_4 (9:1) done at 2300 Pa. by Imanaka et al. (2004)[?] and our experiments is the peaks located around 2090 cm^{-1}.

Why we use different initial reactants, replacing N_2 by NH_3 but we may get similar residues? The similarities during formation of atomic nitrogens when breaking N_2 bonds in nitrogen and NH bonds in ammonia give rise to this result. When photon energy is enough to break both NH bond and N_2 bond, similar experimental residues forms. Our results implies that the residues formed on Charon is similar to what we found on Titan, although their formation environments differs from gaseous phase with N_2 dominating to solid phase with NH_3.

After CH_4+NH_3 = 1:5, 1:10 and 1:20 experiments, we notice that two new bonds are formed. One at 1721 cm^{-1} and another at 1286 cm^{-1}. These two peaks are due to MCT detector self-contamination. When we stopped adding liquid nitrogen, molecules stick onto MCT detector will be free out. They sticked onto our detector and hence produced these two peaks. Hence, we may conclude that the residues produced by CH_4+NH_3 with different ratios are the same.

2.6   Conclusion

The main product of VUV and EUV irradiated CH_4+NH_3 ice mixtures are C_2H_6 and CN^-. C_3H_8 is also produced by C_2H_6 or C_2H_2. We did several investigations towards CH_4+NH_3 ice mixtures. First, by changing ratio of CH_4 and NH_3 in the ice mixture, CN^- production is more effective in NH_3 dominated ice mixtures where C_2H_6 dominates in CH_4 dominated ice mixtures. Second, by changing the photon source to EUV irradiation, the yield of C_3H_8 increases. The effective formation of
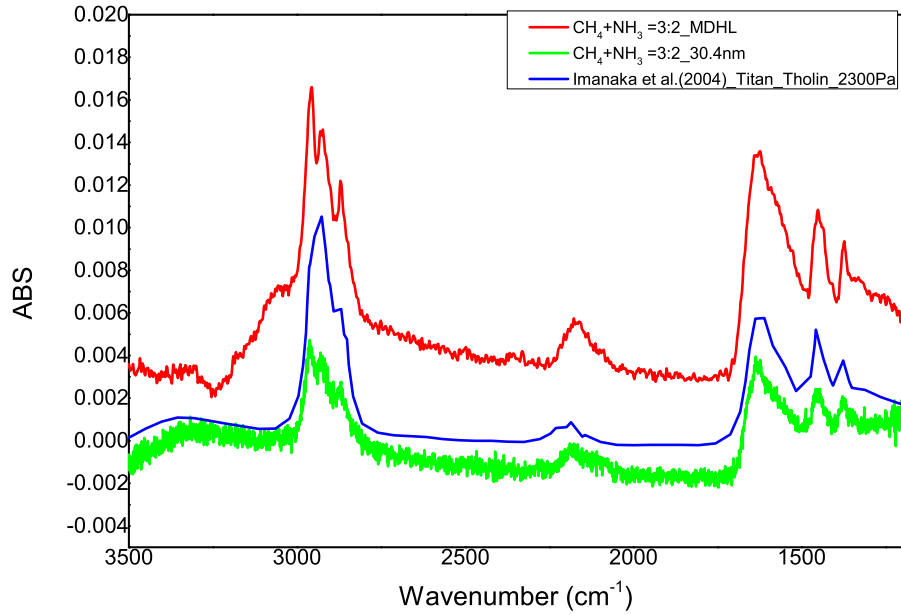
Figure 2.15: The IR spectrum of residues in after $CH_4+NH_3 = 3:2$ experiments and the accumulate residues after MDHL experiments and NSRRC experiments.

C_3H_8 was not produced by C_2H_6 but by C_2H_2 and CH_4 because the ratio of $C_3H_8 : C_2H_6$ increases. This suggests that the CH_2 or CH fragmentation from CH_4 increases when photon energy increases. By studying the production efficiencies, the difference in photo-production yield is mainly caused by the reduction in photo-destruction cross-section in the reactants. Thirdly, by comparison with electron irradiation experiments, electron irradiation has a smaller absorption cross-sections, the percentage of yield is also smaller than VUV irradiated ice mixtures with similar ice thicknesses. Finally, we compared our residues obtained with laboratory produced Taitan tholins, the similar infra-red spectrum shows a similar functional groups in residues. Our result implies that the tholin on Charon should be similar to the tholin formed on Titan.

3. Astrophysical Implications

In this text, we look at effects The main source to irradiating the dark side of Charon is Lyα reflected by interplanetary medium [**?**]. Other sources included energetic ions in solar wind, which mainly consist of H$^+$, He$^+$, He^{++} and O^{2+} etc. originated from solar corona or IPM. These ions also reflect solar irradiation to the dark side of Charon. Among sources focused on He II irradiation as it is 3 toĂŞ 20 times more intense than He I during a solar flare. As the intensity varies with solar activities, it is difficult to estimate the dose onto Charon. Besides, electronic flux is also present in solar wind but it is one order of magnitude lower than proton flux. The flux for energetic electrons observed at the 1 A. U. position is available (http://www.swpc.noaa.gov/products/goes-electron-flux). Although electron flux is much less important than Ly-α, and their flux varies, we also compare the electron irradiation experiment done by Ki ice mixtures.

3.1 Cyanide ion produced by photon source and electron source

We study the ice mixtures in which CH$_4$ is dominated and compare the efficiencies in CN$^-$ formation by electrons and VUV irradiations. Comparing our CN$^-$ obtained after infinitely long exposure, 13 – 16 ML of CN$^-$ was obtained by electron irradiation depending on which equation they choose to fit. In our MDHL experiments, we have 14.8 ML of CN$^-$. However, Kim and Kaiser (2011) adopted the CN$^-$ absorption coefficient measured by Georgieva and Velcheva (2006) to be 3.7×10^{-18} cm molecule^{-1}, which is 4.86 times smaller. We do not adopt this absorption coefficient because it violates the carbon balance that number of CN$^-$ produced will be larger than CH$_4$ consumption. If we adopted

the same absorption coefficient, the production yield of CN⁻ should be multiplied by 4.86. Therefore, our yield is 72 ML of CN^-. Regarding percentage of NH_3 (limiting reactant), Kim and Kaiser has 5 - 6 % yield where we have 12 % yield if we adopted the same absorption coefficients.

Note that Kim and Kaiser kim have ice thickness (CH_4 = 610 ML, NH_3= 260 ML) while we have thicker ices (CH_4 = 900 ML, NH3= 600 ML). Therefore, we calculate the percentage of photons absorbed by CH_4+NH_3 ice mixtures under VUV irradiation. Substituting cross-sections measured by Cruz-Diaz et al. (2014) and the spectrum of our MDHL and substitute them into Beer's law, CH_4+NH_3 = 3:2 ice mixtures can absorb more than 99 % of light when thickness of CH4 and NH3 equals

In electron irradiation experiments of Kim and Kaiser (2011)[?], the energy transferred to CH_4 + NH_3 ice mixtures is by linear electron transfer (LET) that 1.3 eV molecule^{-1} was absorbed by the ice in 90 minutes. They get flattened at 20 minutes' irradiation, with fluence of 2.0×10^{14} electrons cm^{-2}. While we got flattened at a dose of 3×10^{17} photons cm^{-2}. Considering the energy of their electron (1.5 keV) and energy of our photons, they got flattened at 3×10^{17} eV cm^{-2} while we get flattened at 27.81×10^{17} eV cm^{-2}. Comparing these energy doses, less electrons are needed to flatten the formation of CN^-.

To conclude, electron irradiation has a smaller absorption cross-sections, the percentage of yield is also smaller than VUV irradiated ice mixtures with similar ice thicknesses.